Landau-Zener tunneling of solitons

Vazha Loladze and Ramaz Khomeriki
Physics Department, Tbilisi State University, Chavchavadze 3, 0128 Tbilisi, Georgia
(Received 15 July 2016; published 12 April 2017)

We consider Landau-Zener tunneling of solitons in a weakly coupled two-channel system, for this purpose we construct a simple mechanical system using two weakly coupled chains of nonlinear oscillators with gradually decreasing (first chain) and increasing (second chain) masses. The model allows us to consider soliton propagation and Landau-Zener tunneling between the chains. It is shown that soliton tunneling characteristics become drastically dependent on its amplitude in nonlinear regime. The validity of the developed tunneling theory is justified via comparison with direct numerical simulations on oscillator ladder system.

DOI: 10.1103/PhysRevE.95.042204

I. INTRODUCTION

When a quantum or classical coupled two-level linear system evolves adiabatically, a whole process follows one of the adiabatic levels, but if velocity of evolution is finite, there always exists probability of nonadiabatic transition between adiabatic levels, this phenomenon is a celebrated Landau-Zener (LZ) tunneling effect [1], which serves as a powerful tool for a simple quantum-mechanical interpretation of various fascinating wave processes in quantum and classical many-body systems. Landau-Zener effect in general is a wave phenomenon and could show up in any properly designed classical system, and as we demonstrate in the present paper, it is valid even in the case of system of coupled oscillators. LZ model has been applied to explain transitions between Bloch bands considering time dynamics of matter waves of Bose-Einstein condensates in optical lattices [2,3] and acoustic waves in layered elastic structures [4]. Later on the same effect of Bloch mode transitions has been extended in spatial domain considering optical systems with a variety of architectures: waveguide arrays with a step in a refractive index [5], arrays with an applied temperature gradient [6], curved wave guides [7], nematic crystals [8], perturbed optical lattice [9], and two-dimensional photonic lattices [10]. These macroscopic phenomena, at the same time, has led to generalizations of original Landau-Zener problem, for instance, nonlinear LZ tunneling inducing asymmetric transitions [11–13], LZ tunneling in multilevel systems [14,15], and Landau-Zener-Bloch oscillations [16] could be quoted among others. One can mention various application proposals for LZ tunneling, such as targeted energy transfer [17] and all optical diode realization [18].

In the present paper we propose a simple mechanical system in order to show a generic nature of soliton tunneling mechanism in any weakly coupled two-channel system, which can be interpreted as LZ tunneling in spatiotemporal domain. As an example, nonlinear oscillator ladder is examined where in tunneling region oscillator masses are varying monotonously (decreasing and increasing along first and second chains, respectively) as presented in Fig. 1. The applicability of the mentioned mechanism could be seen in system of weakly coupled photonic wave guides, for Bose-Einstein condensates in two parallel closely placed photonic lattices, two coupled spin chains (either classical or quantum) could be also examined, and even weakly coupled completely different media, for instance, ferroelectric and ferromagnetic quasi-one-dimensional systems, could be considered. In the latter case magnetic soliton will transform into electric one or viceversa in multiferroic nanostructures [19].

II. THE MODEL

In order to support generic idea of soliton LZ tunneling we use a most celebrated oscillator system model, namely two weakly coupled Fermi-Pasta-Ulam chains [20], which consist of three parts (Fig. 1). Two ends of the ladder are used as input and output and they consist of two weakly coupled FPU chains, where at the input all oscillators have masses M in upper chain and m in lower one, while, on the other hand, at the output we have masses m and M in upper and lower chains, respectively. The oscillator masses in the tunneling region depends on oscillator position via linear law. FPU oscillator ladder with such a mass distribution could be presented as follows:

$$m_1(n)\ddot{u}_n = k_1(u_{n+1} + u_{n-1} - 2u_n) + k_3(u_{n+1} - u_n)^3 + k_3(u_{n-1} - u_n)^3 + k(w_n - u_n), \quad (1)$$

$$m_2(n)\ddot{w}_n = k_1(w_{n+1} + w_{n-1} - 2w_n) + k_3(w_{n+1} - w_n)^3 + k_3(w_{n-1} - w_n)^3 + k(u_n - w_n), \quad (2)$$

where u_n and w_n are displacements of nth oscillator in upper and lower chains, respectively. We choose mass distribution in the tunneling region,

$$m_1(n) = m_0(1 - \alpha n), \qquad m_2(n) = m_0(1 + \alpha n), \quad (3)$$

such that $m_1(-N/2) = m_2(N/2) = M$ and $m_1(N/2) = m_2(-N/2) = m$, where in tunneling region index n varies in the limits $-N/2 < n < N/2$; m_0 is an oscillator mass in the middle of ladder and α stands for a mass gradient coefficient; k_1 is linear and k_3 is nonlinear coupling stiffness of springs connecting the oscillators of the same chain, while k is a weak coupling constant between oscillators in different chains. It should be especially mentioned that relative difference of masses between different ends of the same chain, i.e., the value $(M - m)/M$ should be small, otherwise analogical to Fressnell reflection effects [21] will take place and one has to take into account both reflection and tunneling processes,

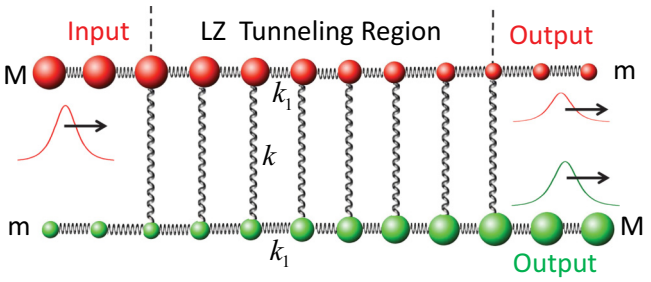

FIG. 1. Schematics for the oscillator ladder system. Soliton is entering through one of the input chains and nonlinear Landau-Zener tunneling is identified via monitoring the soliton amplitudes at the output chains. k and k_1 are interchain and intrachain linear coupling constants and oscillator masses change from M to m in the upper chain and viceversa in the lower chain.

which makes difficult clear identification of manifestations of LZ tunneling.

By introducing dimensionless time variable and redefining parameters it is possible to choose $m_0 = k_1 = 1$. Working in this setup we are seeking the solution in the form of slow space-time modulation of plane waves:

$$u_n = \frac{A(\xi,\epsilon n)}{2} e^{i(\omega t - pn)} + \text{c.c.},$$
$$w_n = \frac{B(\xi,\epsilon n)}{2} e^{i(\omega t - pn)} + \text{c.c.}, \quad \xi = \epsilon(n - vt), \qquad (4)$$

where $\epsilon \ll 1$ is a small expansion parameter. Collective slow variable ξ has been introduced and $v = d\omega/dp = \sin p/\omega$ stands for a group velocity. Now we suppose that $\alpha n \lesssim \epsilon$, $k \sim \epsilon$, and $k_3 \sim \epsilon$. Then in the zero approximation over ϵ substituting Eq. (4) into Eqs. (1) and (2), one automatically gets dispersion relation for plane waves $\omega^2 = 2(1 - \cos p)$. While in the next approximation over ϵ making simple phase modification for A and B, we obtain the following equations:

$$-i\frac{\partial A}{\partial n} = \alpha' n A - \kappa B + 2r|A|^2 A, \qquad (5)$$
$$-i\frac{\partial B}{\partial n} = -\alpha' n B - \kappa A + 2r|B|^2 B, \qquad (6)$$

with gradient coefficient $\alpha' = \omega^2\alpha/(2\sin p)$, coupling constant $\kappa = k/(2\sin p)$, and nonlinearity $r = 3k_3(\cos p - 1)^2/(4\sin p)$. Substituting $A \sim e^{i\beta n}$ and $B \sim e^{i\beta n}$ into Eqs. (5) and (6), it is easy to determine adiabatic levels β for fixed n and one obtains quartic equation,

$$(\alpha' n\beta)^2 = (\beta^2 - \kappa^2)(r\mathcal{F} - \beta)^2, \qquad (7)$$

where $\mathcal{F}(\xi) = |A|^2 + |B|^2$ is a conserved quantity for fixed ξ.

III. LINEAR LIMIT

In the case of vanishing nonlinearity $k_3 \to 0$ ($r \to 0$) Eqs. (5) and (6) reduce exactly to Landau-Zener model [1] in the spatial domain. In the same limit, Eq. (7) gives symmetric adiabatic levels $\beta = \pm\sqrt{\kappa^2 + (\alpha' n)^2}$ displayed in Figs. 2(c) and 2(e). According to general LZ formula [1], having at $n \to -\infty$ the values $A = 1$ and $B = 0$, transition probability

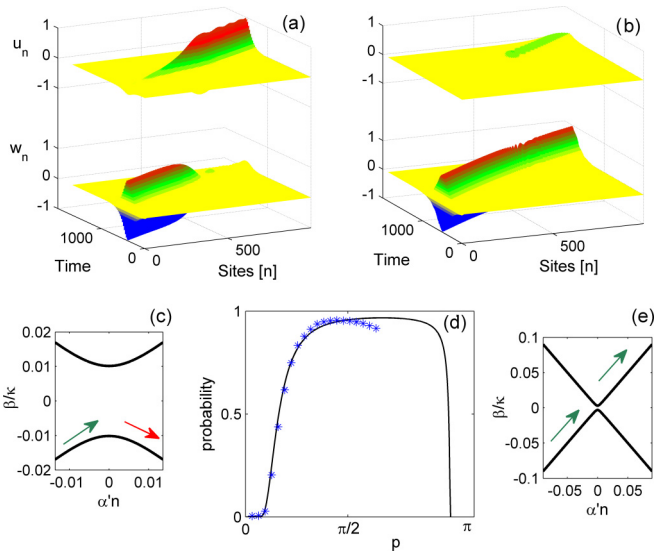

FIG. 2. Result of numerical simulation on the initial model system Eqs. (1) and (2) in linear limit with mass distribution Eq. (3), presented schematically in Fig. 1. Upper surface plots (a) and (b) represent linear wave-packet dynamics injected into the lower chain. Carrier wave numbers are $p = 0.3$ and $p = \pi/2$ in (a) and (b) graphs, respectively. Graph (d) displays analytical dependence of tunneling probability on carrier wave number given by LZ Eq. (8) (solid curve), while stars are results of numerical simulations. Graphs (c) and (d) represent adiabatic and diabatic regimes in linear limit $k_3 \to 0$, corresponding to the cases in the surf plots (a) and (b), respectively. We use the following parameters for the simulations and comparison: keeping intrachain coupling constant equal to unity we choose interchain coupling as $k = 0.006$ and gradient coefficient as $\alpha = 6.5 \times 10^{-4}$. Masses at ultimate ends of the ladder are fixed as $m = 1.09$ and $m = 0.91$.

is expressed as

$$P = \exp\left(-\frac{\pi\kappa^2}{\alpha'}\right) = \exp\left(-\frac{\pi k^2}{2\omega^2\alpha\sin p}\right). \qquad (8)$$

In particular, this means that if according to Eq. (4) one has modulated plane wave distribution at fixed $\xi = \xi_0$ and $n = -\infty$, such that $A(\xi = \xi_0, n = -\infty) = A_0$ and $B(\xi = \xi_0, n = -\infty) = 0$, then Eq. (7) allows us to construct the tunneling amplitudes at $n = \infty$ and the same $\xi = \xi_0$ as follows: $|A(\xi = \xi_0, n = \infty)|^2 = P|A_0|^2$ and $|B(\xi = \xi_0, n = \infty)|^2 = (1 - P)|A_0|^2$.

As a result, taking initially some localized wave function of collective variable ξ, the wave will propagate through tunneling region and at the output the amplitudes should follow to LZ transition probability Eq. (7). Particularly, we inject at the input modulated wave via oscillating ultimate left end of the ladder as follows: $u_0(t) = \cos(\omega t)/\cosh(t/L)$, $w_0(t) = 0$ or $u_0(t) = 0$, $w_0(t) = \cos(\omega t)/\cosh(t/L)$ with $L = 80$ (L should be large in order to have small spreading effects) and monitor wave-packet amplitudes in both chains at the output. Figure 2 shows that in the range $0 < p \lesssim \pi/2$, numerical experiment almost repeats theoretical curve of the dependence of tunneling probability on the carrier wave number of the injected wave-packet p [see Fig. 2(d)]. Particularly, the process is strongly symmetric, i.e., injecting the wave packet into

upper (lower) chain and keeping pinned lower (upper) chain, tunneling characteristics for both processes are exactly the same as it should follow from original LZ model. On the other hand, changing carrier wave number of the injected wave packet from $p = 0.3$ to $p = \pi/2$, one monitors transition from almost complete switch [Fig. 2(a)] toward almost complete transmission [Fig. 2(b)], according to general formula Eq. (8). However, for large wave numbers $p \approx \pi$, the correspondence is violated because of the reflection processes due to the following reasons: for the mentioned carrier wave numbers, the wave packet has a small group velocity and therefore Fressnell's reflection is in force, moreover as one goes closer to the Brillouin zone boundary, the wave packet injected into the upper chain cannot propagate in the same chain due to resonance mismatch. As a result, tunneling is no more symmetric and there appear quantitative and qualitative differences compared with the original Landau-Zener model.

IV. NONLINEAR CASE

Turning back to the nonlinear case in frames of approximate description of Eqs. (5) and (6) we should deal with quartic equation for β level distribution Eq. (7). Corresponding curves in strongly nonlinear regime (defined by condition $r\mathcal{F} > \kappa$) are displayed in Fig. 3(b) and evidently there is definite asymmetry: Particularly, in the case of small gradient constants α, adiabatic regime could be still realized injecting wave packet into the upper chain, then the system follows the upper curve of the graph (b) in Fig. 3, while injecting the wave packet into the lower chain, the dynamics is always diabatic even in vanishing gradient case $\alpha \to 0$ as it is evident from the lower curve of the same graph. Further, we will consider only such strongly nonlinear cases $r\mathcal{F} > \kappa$ and examining soliton splitting while passing through the tunneling region of the ladder.

In order to investigate soliton LZ tunneling process we employ a weakly nonlinear soliton solution in a single oscillator chain,

$$G_n(\xi) = \frac{G\cos(\omega t - pn)}{\cosh(\xi)}, \quad \xi = \frac{n - vt}{\Lambda}, \tag{9}$$

where G and Λ are soliton amplitude and width, respectively, and the latter is defined from the relation $1/\Lambda = G\omega\sqrt{3k_3/2}$. Let us mention that the envelope of Eq. (9) is associated [22] with exactly one soliton solution of the nonlinear Schrödinger equation.

V. NUMERICAL SIMULATIONS AND JUSTIFICATION OF THEORETICAL MODEL

Now we shall demonstrate all the procedures step by step on the particular examples presented in Figs. 3 and 4, where injection of the soliton into upper and lower chains, respectively, has been considered. In both cases we inject the soliton Eq. (9) with carrier wave number $p = \pi/2$ (thus carrier frequency is $\omega = \sqrt{2(1 - \cos p)} = \sqrt{2}$) and we take interchain coupling and nonlinearity constants as follows: $k = 0.01$, $k_3 = 0.015$, while the mass gradient in the tunneling region is $\alpha = 0.00008$. First we choose the input signal with a unit amplitude soliton Eq. (9) in the upper chain, i.e., $G_0^U = 1$ and $G_0^L = 0$. Corresponding surface plot and level distribution

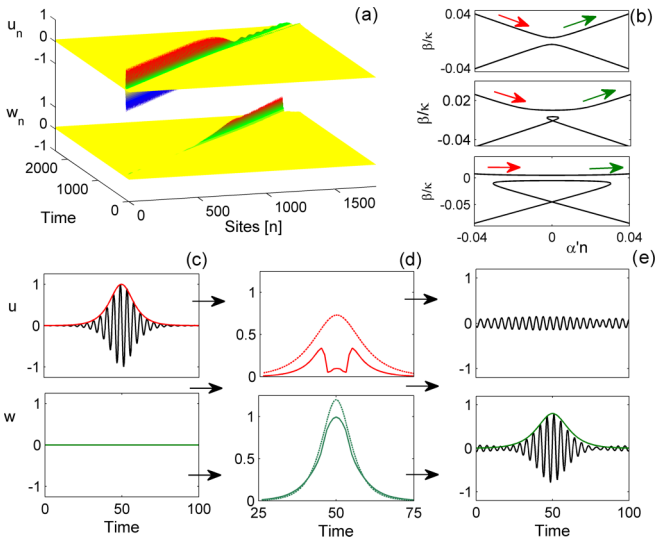

FIG. 3. (a) surface plot of simulations on the initial model Eqs. (1) and (2) when unit amplitude soliton is injected in the upper chain. Panel (b) displays adiabatic dynamic associated with this process where the curves are taken solving quartic Eq. (7) and arrows indicate that soliton is switching to the lower chain. (c, d) graphs represent soliton LZ tunneling process. Particularly, in graph (c) the shape of injected soliton with envelope function Eq. (10) in the upper chain is shown (while lower input is pinned). In graph (d) we present resulting envelopes (solid lines) after tunneling derived from model Eqs. (5) and (6). Dashed lines indicate constructed regular soliton envelopes Eq. (9) with the same width at half maximum as ones plotted by solid lines. Panel (e) shows formed output signal profiles followed from direct numerical simulations on Eqs. (1) and (2) indicated by solid lines. Analytically computed envelope according to scheme Eq. (12) in the lower chain is given by dashed line, while in upper chain the envelope does not exist since the soliton does not form. The following parameters are used for the calculations: nonlinearity coefficient is $k_3 = 0.015$, while interchain constant takes the value $k = 0.01$, gradient is $\alpha = 0.00008$, and we take carrier wave number $p = \pi/2$.

is presented in Figs. 3(a) and 3(b), while explicit form of the soliton shapes in upper and lower chains is presented in graph Fig. 3(c). This means that according to the developed scheme of nonlinear LZ tunneling one has the following values for the envelope variables A and B from Eq. (4) at the input $n \to -\infty$:

$$A(\xi, n \to -\infty) = \frac{1}{\cosh(\xi)}, \quad B(\xi, n \to -\infty) = 0. \tag{10}$$

For each value of variable ξ the input values of Eq. (10) undergo evolution following to the nonlinear LZ Eqs. (5) and (6), getting after tunneling process the values $A(\xi, n \to \infty)$ and $B(\xi, n \to \infty)$, which do not have the regular soliton shape any more as it is evident from graph Fig. 3(d) (their shapes in both chains are plotted as solid lines). The obtained envelope distributions $A(\xi, n \to \infty)$ and $B(\xi, n \to \infty)$ could be now considered as initial conditions for the associated nonlinear Schrödinger equation, and the problem becomes exactly solvable [23–26]. In particular, one is able to say whether the soliton will be formed or decayed. Moreover, one can predict the soliton amplitude and shape at the output of each chain explicitly in a good approximation.

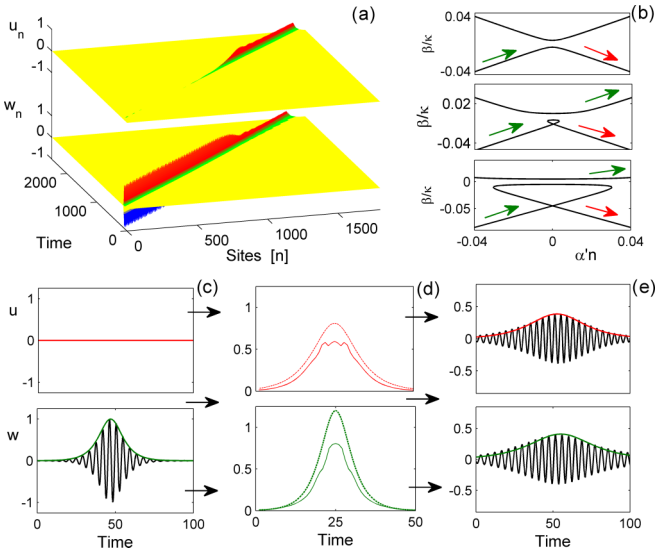

FIG. 4. (a) Results of direct numerical simulations when unit amplitude soliton is injected into the lower chain. Panel (b) displays diabatic dynamic associated with the process and arrows indicate that part of the input soliton switches to the upper chain while another part stays in the same chain. (c) The shape of injected soliton in the lower chain is shown (while upper input is pinned). Panel (d) represents resulting envelopes (solid lines) after tunneling derived from model Eqs. (5) and (6). Dashed lines indicate constructed regular soliton envelopes Eq. (9) with the same width at half maximum as ones plotted by solid lines. Panel (e) shows formed output soliton profiles followed from direct numerical simulations on Eqs. (1) and (2) indicated by solid lines. Analytically computed envelopes according to scheme Eq. (12) in both chains are given by dashed lines. The parameters are the same as in Fig. 3.

In this connection, first of all, one should mention that it is crucial to determine characteristic amplitudes and widths of the obtained distributions $A(\xi,n\to\infty)$ and $B(\xi,n\to\infty)$. Measuring their amplitudes in Fig. 3(d), we get the following values: $G_1^U = \mathrm{Max}[A(\xi,n\to\infty)] = 0.995$ and $G_1^L = \mathrm{Max}[B(\xi,n\to\infty)] = 0.34$, while measuring their width at half maximum we get $\Lambda_U = 11$ and $\Lambda_L = 18$. Next we should plot the regular soliton profile Eq. (9) characterized by the same width at half maximum. For our parameters the width of the regular soliton is defined from the relation $1/\Lambda_0 = G\sqrt{3k_3}$, and thus the amplitudes of corresponding regular solitons are given by the following expressions:

$$G_2^U = \frac{\mathrm{acosh}(2)}{\Lambda_U\sqrt{3k_3}} = 0.73, \quad G_2^L = \frac{\mathrm{acosh}(2)}{\Lambda_L\sqrt{3k_3}} = 1.2. \quad (11)$$

The latter regular solitons are displayed in both chains by dashed lines in Fig. 3. Comparing now the amplitudes G_1^U and G_1^L with G_2^U and G_2^L, respectively, one can make definite predictions about formation of the solitons in each chain. In particular, as far as in the upper chain $G_1^U/G_2^U < 1/2$ the soliton will not form at the output, while in the lower chain the soliton formation condition $G_1^L/G_2^L > 1/2$ is satisfied and its amplitude could be computed approximately as follows:

$$G_L = 2G_2^L\left(\frac{G_1^L}{G_2^L} - \frac{1}{2}\right) = 0.8. \quad (12)$$

Then it is easy to recover the full shape of the solitons according to Eq. (9), and this gives excellent fit with the results of direct numerical simulations on initial set of Eqs. (1) and (2) as is evident from Fig. 3(e).

Now we proceed with the similar arguments in order to understand soliton spitting behavior presented in Fig. 4(a), where unit amplitude soliton Eq. (9) is injected into the lower chain. In this case the dynamics follows lower level line of Fig. 4(b), and therefore the process is strongly diabatic. As a result, the picture is quite different from what we have seen in case of soliton injection into the upper chain (see Fig. 3). Following the above developed procedure, one should measure characteristic amplitudes of solid line curves in Fig. 4(d). We get following values: $G_1^U = 0.805$, $G_1^L = 0.6$, while for their widths at half maximum we get $\Lambda_U = 5.6$ and $\Lambda_L = 8$. Next, as in the previous case, we should plot the regular soliton profiles Eq. (9) characterized by the same width at half maximum and similar to Eq. (11) calculations give the regular soliton amplitude values $G_2^U = 1.18$ and $G_2^L = 0.82$. Both associated regular solitons are displayed by dashed lines in Fig. 4. Comparing now the amplitudes G_1^U and G_1^L with G_2^U and G_2^L, respectively, one can conclude that soliton formation condition is fulfilled both in upper and lower chains and the solitons will form with amplitudes easily determined from the relation Eq. (12). Thus, we get $G^U = 0.42$ and $G^L = 0.37$. Then one recovers solitons according to Eq. (9) and compares with the results of the direct numerical simulations that are done in Fig. 4(e).

VI. CONCLUSIONS

Concluding, we have interpreted soliton-splitting phenomenon in a gradiented two-channel weakly coupled system as nonlinear Landau-Zener tunneling and made comparison between direct numerical simulations and simple analytical scheme in case of oscillator ladder. This correspondence becomes worse in the case of large relative mass differences and/or small soliton propagation velocities. This is due to Fresnel's reflection, which has not been taken into account. The investigations of interplay between Fresnel's reflection and Landau-Zener tunneling will be a subject of our further studies.

ACKNOWLEDGMENTS

The authors acknowledge financial support from Georgian SRNSF (Grants No. FR/25/6-100/14 and No. 216662). R.Kh. is supported in part by travel grants from Georgian SRNSF and CNR, Italy (Grant No. 04/24) and CNRS, France (Grant No. 04/01).

APPENDIX

LZ tunneling region of our system is described by following equation:

$$\begin{aligned} m_0(1-\alpha n)\ddot{u}_n &= k_1(u_{n+1}+u_{n-1}-2u_n) + k_3(u_{n+1}-u_n)^3 \\ &\quad + k_3(u_{n-1}-u_n)^3 + k(w_n-u_n), \\ m_0(1+\alpha n)\ddot{w}_n &= k_1(w_{n+1}+w_{n-1}-2w_n) + k_3(w_{n+1}-w_n)^3 \\ &\quad + k_3(w_{n-1}-w_n)^3 + k(u_n-w_n). \end{aligned} \quad (A1)$$

If we redefine parameters, $k_3 \equiv \frac{k_3}{k_1} k \equiv \frac{k}{k_1}$, and introduce dimensionless time, $t \equiv t\sqrt{\frac{k_1}{m_0}}$, we obtain

$$\begin{aligned}(1-\alpha n)\ddot{u}_n &= (u_{n+1}+u_{n-1}-2u_n)+k_3(u_{n+1}-u_n)^3 \\ &\quad +k_3(u_{n-1}-u_n)^3+k(w_n-u_n), \\ (1+\alpha n)\ddot{w}_n &= (w_{n+1}+w_{n-1}-2w_n)+k_3(w_{n+1}-w_n)^3 \\ &\quad +k_3(w_{n-1}-w_n)^3+k(u_n-w_n). \end{aligned} \tag{A2}$$

Let us seek solutions of Eq. (2) as follows:

$$\begin{aligned} u_n &= \frac{A(\xi,\epsilon n)}{2}e^{i(\omega t-pn)}+\text{c.c.}, \\ w_n &= \frac{B(\xi,\epsilon n)}{2}e^{i(\omega t-pn)}+\text{c.c.}, \\ \xi &= \epsilon(n-vt), \end{aligned} \tag{A3}$$

where $\epsilon << 1$, $v = \frac{\sin p}{w}$, and we suppose that $\alpha n \lesssim \epsilon$, $k \sim \epsilon$, $k_3 \sim \epsilon$.

In the zero approximation over ϵ, we have a dispersion relation:

$$\omega^2 = 2(1-\cos p), \tag{A4}$$

while in the linear approximation over ϵ, we get

$$\begin{aligned} -i\frac{\partial A}{\partial n} &= \alpha' nA-\kappa(B-A)+2r\mid A\mid^2 A, \\ -i\frac{\partial B}{\partial n} &= -\alpha' nB-\kappa(A-B)+2r\mid B\mid^2 B, \\ \alpha' &= \frac{\alpha\omega^2}{2\sin p}, \quad \kappa = \frac{k}{2\sin p}, \quad r = \frac{3}{4}(\cos p-1)^2 k_3. \end{aligned} \tag{A5}$$

With a phase transformation, $A/B = A/Be^{i\kappa n}$, we arrive to the equations

$$\begin{aligned} -i\frac{\partial A}{\partial n} &= \alpha' nA-\kappa B+2r\mid A\mid^2 A, \\ -i\frac{\partial B}{\partial n} &= -\alpha' nB-\kappa A+2r\mid B\mid^2 B. \end{aligned} \tag{A6}$$

This equation coincides with Eqs. (5) and (6) from the main text.

Now let us define adiabatic levels. Substituting $A/B = A/Be^{i(\beta+r\mathcal{F})n}$ into Eq. (6) (where $\mathcal{F} = |A|^2+|B|^2$ is constant for fixed ξ_0), we get the following system of equations:

$$\begin{aligned} \beta A &= \alpha' nA-\kappa B+r(\mid A\mid^2-\mid B\mid^2)A, \\ \beta B &= -\alpha' nB-\kappa A-r(\mid A\mid^2-\mid B\mid^2)B. \end{aligned} \tag{A7}$$

From Eq. (7) we can determine

$$\mid A\mid^2-\mid B\mid^2 = \frac{\alpha' n\mathcal{F}}{\beta-r\mathcal{F}}, \tag{A8}$$

combining Eqs. (7) and (8), we have

$$\begin{aligned} \left(\beta-\frac{\alpha' n\beta}{\beta-r\mathcal{F}}\right)A+\kappa B &= 0, \\ \kappa A+\left(\beta+\frac{\alpha' n\beta}{\beta-r\mathcal{F}}\right)B &= 0. \end{aligned} \tag{A9}$$

Equations (9) are linear homogenous equations for A and B. We have nontrivial solutions of Eq. (9) if

$$(\alpha' n\beta)^2 = (\beta^2-\kappa^2)(r\mathcal{F}-\beta)^2. \tag{A10}$$

This quartic equation determines adiabatic levels β for fixed n.

[1] L. D. Landau, Phys. Z. Sowjetunion **2**, 46 (1932); G. Zener, Proc. R. Soc. London A **137**, 696 (1932).
[2] B. P. Anderson and M. Kasevich, Science **282**, 1686 (1998).
[3] M. Cristiani, O. Morsch, J. H. Müller, D. Ciampini, and E. Arimondo, Phys. Rev. A **65**, 063612 (2002).
[4] H. Sanchis-Alepuz, Y. A. Kosevich, and J. Sanchez-Dehesa, Phys. Rev. Lett. **98**, 134301 (2007); L. Gutierrez, A. Diaz-de Anda, J. Flores, R. A. Mendez-Sanchez, G. Monsivais, and A. Morales, *ibid.* **97**, 114301 (2006).
[5] R. Khomeriki and S. Ruffo, Phys. Rev. Lett. **94**, 113904 (2005).
[6] H. Trompeter, T. Pertsch, F. Lederer, D. Michaelis, U. Streppel, A. Brauer, and U. Peschel, Phys. Rev. Lett. **96**, 023901 (2006).
[7] F. Dreisow, A. Szameit, M. Heinrich, S. Nolte, A. Tunnermann, M. Ornigotti, and S. Longhi, Phys. Rev. A **79**, 055802 (2009).
[8] A. Fratalocchi and G. Assanto, Opt. Express **14**, 2021 (2006).
[9] A. Fratalocchi and G. Assanto, Phys. Rev. A **75**, 013626 (2007).
[10] H. Trompeter, W. Krolikowski, D. N. Neshev, A. S. Desyatnikov, A. A. Sukhorukov, Y. S. Kivshar, T. Pertsch, U. Peschel, and F. Lederer, Phys. Rev. Lett. **96**, 053903 (2006).
[11] B. Wu and Q. Niu, Phys. Rev. A **61**, 023402 (2000).
[12] J. Liu, L. Fu, B.-Y. Ou, S.-G. Chen, D. I. Choi, B. Wu, and Q. Niu, Phys. Rev. A **66**, 023404 (2002).
[13] X.-Z. Liu, D.-P. Tian, and B. Chong, Physica B (Amsterdam) **490**, 1 (2016).
[14] A. V. Shytov, Phys. Rev. A **70**, 052708 (2004).
[15] R. Khomeriki, Eur. Phys. J. D **61**, 193 (2011).
[16] R. Khomeriki and Sergej Flach, Phys. Rev. Lett. **116**, 245301 (2016).
[17] M. A. Hasan, Y. Starosvetsky, A. F. Vakakis, and L. I. Manevitch, Physica D (Amsterdam) **252**, 46 (2013).
[18] R. Khomeriki, Phys. Rev. A **82**, 013839 (2010).
[19] L. Chotorlishvili, R. Khomeriki, A. Sukhov, S. Ruffo, and J. Berakdar, Phys. Rev. Lett. **111**, 117202 (2013).
[20] E. Fermi, J. Pasta, S. Ulam, and M. Tsingou, in *The Many-Body Problems*, edited by D. C. Mattis (World Scientific, Singapore, 1993); *The Fermi-Pasta-Ulam Problem: A Status Report*, edited by G. Gallavotti (Springer, New York, 2008).
[21] A. Szameit, H. Trompeter, M. Heinrich, F. Dreisow, U. Peschel, T. Pertsch, S. Nolte, F. Lederer, and A. Tünnermann, New J. Phys. **10**, 103020 (2008).
[22] R. Khomeriki, Phys. Rev. E **65**, 026605 (2002).
[23] T. Iizuka and M. Wadati, J. Phys. Soc. Jpn. **61**, 3077 (1992).
[24] T. Iizuka, H. Amie, T. Hasegawa, and C. Matsuoka, J. Phys. Soc. Jpn. **65**, 3237 (1996).
[25] J. Satsuma and N. Yajima, Prog. Theor. Phys. Suppl. **55**, 284 (1974).
[26] L. Tkeshelashvili, Phys. Rev. A **86**, 033836 (2012).